Received 16 November 2025; Accepted 17 December 2025
https://doi.org/10.48612/letters/2026-1-30-36
https://elibrary.ru/fweunj

Computational study of fluorinated nanodiamonds: Thermodynamics, electronic structure and interaction with PMMA

K. P. Katin†[1], V. A. Bryzgalov[2,3], D. D. Nikolaev[1], K. S. Grishakov[1], P. F. Kartsev[1], M. M. Maslov[1]

†KPKatin@yandex.ru

[1]National Research Nuclear University MEPhI, Moscow 115409, Russia
[2]Ufa University of Science and Technology, Ufa 450076, Russia
[3]Institute of Metal Superplasticity Problems, Ufa 450001, Russia

Abstract: Fluorinated nanometer-scaled diamond particles (NDs) $C_{26}F_{32}$, $C_{84}F_{64}$ and $C_{148}F_{96}$ have been theoretically investigated using the dispersion-corrected density functional theory. We justify that fluorinated NDs are more thermodynamically stable than fluorinated fullerenes of comparable size due to the stronger C-F bonds. Consequently, NDs are also more resistant to defluorination. The differences in lengths and energies of C-F bonds formed on the NDs edges and surfaces are discussed in details. We observe that fluorine atoms contribute significantly to both frontier molecular orbitals of fluorinated NDs. The HOMO-LUMO gap has a tendency to decrease with the ND size. The electron density transfer from the carbon core to the fluorine shell is found to be about 0.1 electrons per fluorine atom. Global optimization of the polymethyl methacrylate (PMMA) + ND configuration have been carried out with the genetic algorithm. A weak interaction of fluorinated NDs with PMMA polymer has been established. The concrete value and sign of the binding energy depends on the ND size. The electronic orbitals of NDs almost do not hybridize with those of the PMMA, so the optical properties of NDs into the polymer matrix remain unchanged. The paper discusses the effect of ND coating with fluorine and other functional groups on the mechanical and optical characteristics of the resulting NDs/polymer composite.

Keywords: nanodiamond, fluorination, PMMA, composite, density functional theory

Acknowledgements: *The reported study was supported by Ministry of Science and Higher Education of the Russian Federation (agreement/grant 075-15-2025-609).*

1. Introduction

Nanodiamonds (NDs) [1] are nanoscale particles composed of sp^3-hybridized carbon atoms. In contrast to fullerenes, NDs exhibit a distinctive atomic configuration, wherein each atom forms four chemical bonds with its neighbors. The thermodynamic stability of NDs has been thoroughly studied and discussed [2]. According to well-known relation, the energy of the bulk diamond exceeds that of bulk graphite by 2.9 kJ/mol under standard conditions [3]. To become a diamond more favorable compared to graphite, very specific conditions (high pressure and high temperature) are required. However, the thermodynamic advantage of graphite over diamond is not valid at the nanoscale. A comparison of graphene-like nanoparticles (fullerenes) and NDs reveals that NDs are thermodynamically competitive for certain nanoparticle sizes. Pioneering study be Barnard et. al predicted the NDs are more stable in 1.9 to 5.2 nm range [2]. In later study [4], the boundaries of this range were refined for different conditions.

In contrast to fullerenes, pristine NDs inevitably possess dangling bonds on their surface. They can be terminated by hydrogen or other functional groups. Since we deal with nanostructures, the termination involves a significant fraction of atoms and influences on the thermodynamics of the entire nanoparticles. Since the activity of surface carbon atoms in NDs and fullerenes are different, terminated groups can change the thermodynamic competitiveness of NDs and fullerenes.

In this study, we have focused on the fluorinated NDs. Although most computational investigation consider more simple hydrogenated systems, fluorinated NDs possess some advantages. They can be easily synthesized from Teflon without external fluorine source [5]. Khabashesku et al. experimentally demonstrated that fluorination results in higher resistance on NDs to graphitization [6]. Zagrebina et al. reported that fluorination leads to high-quality NDs without sp^2-hydrohenized shells [7]. Nesvizhevsky et al. observed reflection of slow neutrons by NDs and proposed a new kind of neutron reflector based on this effect [8]. In addition, the high electronegativity of fluorine leads to a redistribution of charges in the particle and changes the NDs reactivity. Moreover, the fluorine nucleus provides a strong NMR signal and chemical shift, facilitating experimental detection and characterization of the fluorinated system [9]. Finally, most carbon nanostructures are used for different applications in their fluorinated forms, including NDs, fullerenes [10], nanotubes [11] and graphene [12]. Fluorinated fullerenes

and graphene are also considered as the promise drugs carriers [13]. This is why we are particular interested in fluorinated NDs.

NDs deserves to be studied not only in its pristine form. They attract attention as components of complex advanced nanomaterials [14–16]. Composites based on NDs and polymers such as acrylate [17,18] or polypropylene [19] are used in various applications. In particular, polymethyl methacrylate (PMMA) is often used as a suitable polymer matrix for NDs [20]. Fouda et al. reported increase in flexural strength, impact strength, and hardness and antifungal activity of PMMA after its doping with NDs [21,22]. Wang et al. fabricated a supercapacitor with record energy density used NDs/PMMA composite [23]. Gad et al. applied similar NDs/PMMA compound for denture repair [24]. Many other applications are available for NDs/PMMA [25].

Indeed, the terminated groups coated the NDs effect on their interaction with the polymer and determine the composite characteristics. Fluorinated NDs interact with PMMA in a different way compared to pristine or hydrogenated NDs. According to Ref. [26], fluorinated C_{60} fullerene possesses twice higher interaction energy with 40 common drugs compared to pristine C_{60} due to hydrogen binding. In this study, we used the density functional theory (DFT) to examine in details the interaction between fluorinated NDs with PMMA. Since PMMA can not form hydrogen bonds, it is expected to slighter interacts with fluorinated NDs. So NDs can keep their identity and optical properties in composites with PMMA.

2. Computational methods

The initial NDs configurations were cut from bulk diamond using the NanoCrystal tool [27]. They were then fixed and fluoridated manually. The edge/surface carbon atoms were passivated by two/one fluorine atoms, so that the total number of their bonds was four. The initial geometries of the NDs + PMMA complexes were generated using the genetic algorithm provided in the ABCluster program [28]. The final optimization of NDs, fullerenes, PMMA, and complexes was carried out using the density functional theory. The PBE/6-31G* technique and D3 dispersion corrections [29] were used, which are important for the non-covalent bonds between NDs and polymer. The DFT calculations were performed in the TeraChem package [30 – 31]. The electronic properties were calculated for the equilibrium geometry. The MultiWfn tool [32] provides post-processing of electron density for deriving electronic properties. ChemCraft provides visualization of the considered electronic systems and their molecular orbitals.

3. Results

3.1. Structure of the fluorinated NDs

A realistic nanoparticle model does not have to be almost spherical. A reasonable model should take into account the energy of the various facets of the crystal from which the nanoparticle is being cut. The NanoCrystal software contains an intrinsic algorithm to take into account the energies of various crystal facets. When generating nanoparticles, we adopted the energies (001), (110), and (111) diamond surfaces presented in Ref. [33]. However, the resulted nanoparticles are still close to spherical, see Fig. S1 (Supplementary material). To take into account the possible dependence on the size of the NDs, three models of different sizes were considered. These are $C_{26}F_{32}$ (Fig. S1a), $C_{84}F_{64}$ (Fig. S1b) and $C_{148}F_{96}$ (Fig. S1c) nanoparticles. Their diameters are approximately 0.8, 1.1, and 1.3 nm, respectively. The number of atoms, the size of the Gaussian basic set, and therefore the amount of the required computer resources increases dramatically with the particle diameter. For this reason, we did not consider larger models.

To present the calculated bond lengths visually, we calculated a radial distribution function (RDF) as shown in Fig. 1. Each peak related to the bond is broadened by a Gaussian function, so we define RDF as

$$RDF(r) = \sum_i \sum_{j>i} \frac{1}{\sqrt{2\pi}\sigma} \exp\left(\frac{-(r - r_{ij})^2}{2\sigma^2} \right) \qquad (1)$$

Here r_{ij} is the interatomic distance, indexes i and j number the atoms and $\sigma = 0.002$ Å. This value probably exceeds the achievable accuracy of the applied DFT approach. However, the adopted σ is small enough to observe the peaks splitting, demonstrated slightly different bond lengths appeared in the considered system. In particular, Fig. 1 clearly shows that there are two typical C-F bond lengths in the system, with peaks at 1.278 and 1.361 Å, respectively. The shorter C-F bonds correspond to the edges of the nanoparticle, where two fluorine atoms attach to each carbon atom. The longer C-F bonds correspond to the nanoparticle surfaces, where only one fluorine atom binds to each carbon atom. The positions of both peaks are almost identical for nanoparticles of different sizes. The ratio of their intensities corresponds to the number of C-F bonds of different types formed on the surfaces and edges of the nanoparticle. Note that the calculated bond lengths are in a good agreement with typical experimental values for C-F bonds, ranging from 1.36 (estimated from neutron scattering) to 1.38 Å (estimated with NMR) [34].

The C-C bonds also have different lengths, as presented in the right part of Fig. 1. The bonds in the nanoparticle core are

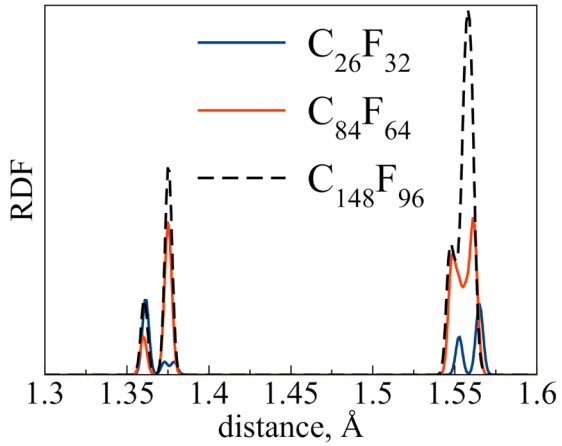

Fig. 1. (Color online) RDF functions for considered models of fluorinated NDs.

slightly longer than that on the surface. Bonds of both types are shorter for larger nanoparticles, see Fig. 1. The intensity ratio is also explained by the different ratio of atoms in the core and on the surface of nanoparticles of different sizes.

3.2. Stability of the fluorinated NDs

There are different ways to evaluate the stability of NDs. The first value relevant to stability is the energy of defluorination E_{df}. We define E_{df} as the energy required to detach a single fluorine atom:

$$E_{df} = E(C_nF_{m-1}) + 0.5E(F_2) - E(C_nF_m). \quad (2)$$

Here $E(C_nF_{m-1})$ and $E(C_nF_m)$ are the total energies of defluorinated and original fluorinated NDs, respectively; $E(F_2)$ is the energy of the isolated fluorine molecule. As mentioned above, there are two types of C-F bonds in NDs. Breaking bonds of different types requires a slightly different amount of energy. Both values of E_{df} for each considered system are presented in Table 1. All E_{df} values are close to 4 eV, so E_{df} is almost independent on ND size. High value of E_{df} shows that fluorinated ND is much more feasible compared to pristine ND and isolated F_2 molecules. As expected, breaking the shorter bond on the ND edge requires ≈0.3 eV more energy compared to longer bond on the ND surface.

For the purpose of the comparison, we also calculate the E_{df} value for fully fluorinated $C_{84}F_{84}$ fullerene with the same formula (2). We obtained the negative value $E_{df} = -1.54$ eV. So, the dissociation of F_2 molecule and subsequent attachment of fluorine atoms to fullerene is energetically unfavorable process. The low value of E_{df} in fullerenes can be explained. It is known that fluorographene is fluorinated on both sides. Such a structure provides near tetrahedral coordination for each carbon atom. However, the inner side of the fullerene is unachievable, so only the outer surface undergoes fluorination. This fact results in weaker C-F binding in fullerenes. Therefore, fluorination of NDs is more energetically feasible compared to fullerene. To clear compare the energies of fluorinated NDs and fluorinated fullerenes, we calculated the ΔE values according to the following formula:

$$\Delta E = E(C_nF_n) + 0.5(m-n)E(F_2) - E(C_nF_m) \quad (3)$$

Here, $E(C_nF_n)$ is the energy of the fluorinated fullerene, $E(F_2)$ is the energy of a fluorine molecule, $n = 32$, 64 or 148 is the number of carbon atoms in the fullerene or ND. Since there is not common C_{148} fullerene, we used the doubled energy of $C_{74}F_{74}$ instead of $E(C_{148}F_{148})$ for $n = 148$ in formula (3). The fullerene cages with common symmetries are considered (C_{26}-D_{3h}, C_{74}-D_{3h}, C_{84}-D_2). In fact, ΔE is the energy required to transform fluorinated ND to fluorinated fullerene (accompanied by the absorption or emission of the required number of the F_2 molecules). The positive values of ΔE confirms that fluorinated ND are more thermodynamically stable compared to fluorinated fullerenes. Therefore, the fluorination changes the thermodynamic order of fullerenes and NDs due to stronger C-F bonds formed by ND.

3.3. Electronic properties of fluorinated NDs

Table 1 also includes the energies of the frontier molecular orbitals, HOMO and LUMO. According to Table 1, the HOMO energy is close to −8 eV for all NDs. However, the LUMO energy is different for systems of different sizes. In general, we observe a decrease in the HOMO-LUMO gap as the size of the nanostructure increases. Such a behavior is typical for most nanosystems and is associated with a decrease in electron localization. The slight non-monotonic variations in the gap width could be related to structural features of certain NDs models considered here. The largest ND shows a gap of about 5 eV, which is somewhat lower than the value for bulk diamond (about 5.5 eV). This difference can be explained by the effect of fluoride. Figure 2 shows the shapes of the frontier molecular orbitals, as well as the total and partial density of electronic states (DOS), reflected the contributions from carbon and fluorine atoms. Figure 2 clear shows that fluorine provides a significant contribution to the HOMO and weaker but not negligible contribution to LUMO of all studied NDs.

Table 1 also shows the averaged partial Lowdin charges for carbon and fluorine atoms. We used Lowdin charges because they are not affected by the electronic basis used, in contrast to the more common Mulliken charges. According to Table 1, the charges of fluorine atoms are negative and close to $-0.1|e|$ (e is the elementary charge) for NDs of all sizes. Carbon atoms have a positive charge, providing electroneutrality of the whole ND. In larger NDs, the proportion of carbon atoms is higher, so their averaged charge decreases with the size of the system, as shown in Table 1. The negative charge of the fluorine shell of a ND should result in its stronger interaction with positively charged parts of other molecules or materials. On the other hand, it can repulse oxygen and other negatively charged atoms with high electronegativity.

3.4. Interaction of fluorinated NDs with PMMA

We used the PMMA model consisting of three monomeric fragments. The broken bonds on the polymer chain ends are passivated with hydrogen, so that the molecular model $C_{16}H_{28}O_6$ are obtained to represent the PMMA. Using finite models allows for calculations with accurate Gaussian basis sets and functionals, whereas the size of

Table 1. Defluorination energy E_{df} and energy difference ΔE calculated with formulas (2) and (3), respectively. Frontier molecular orbitals HOMO and LUMO and averaged partial Lowdin charges of carbon q_C and fluorine q_F atoms are also presented for $C_{26}F_{32}$, $C_{84}F_{64}$ and $C_{148}F_{96}$ NDs.

	E_{df}, eV	ΔE, eV	HOMO, eV	LUMO, eV	gap, eV	q_C	q_F
$C_{26}F_{32}$	3.79/4.07	21.50	−8.14	−1.26	6.28	0.12	−0.10
$C_{84}F_{64}$	3.86/4.08	41.36	−7.93	−3.07	4.86	0.08	−0.11
$C_{148}F_{96}$	3.81/4.06	25.52	−7.75	−2.78	4.97	0.07	−0.10

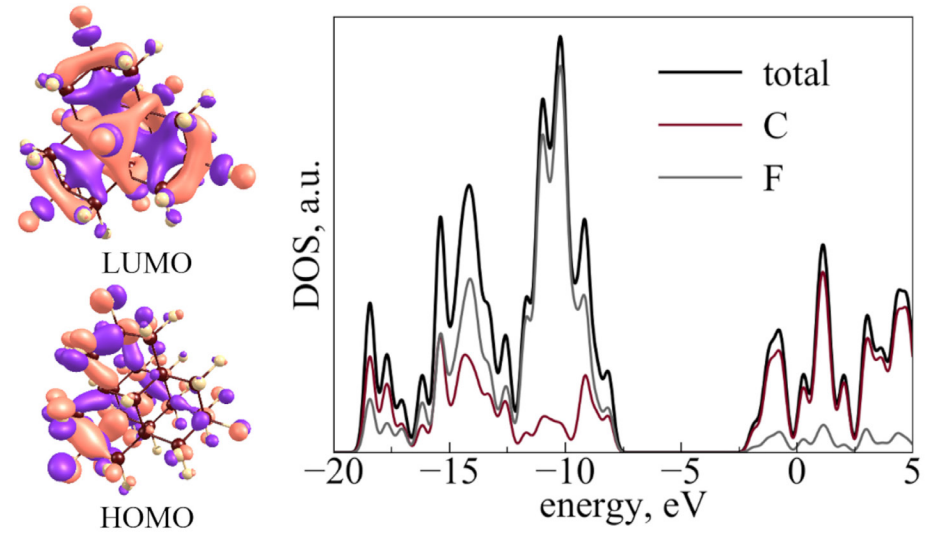

a

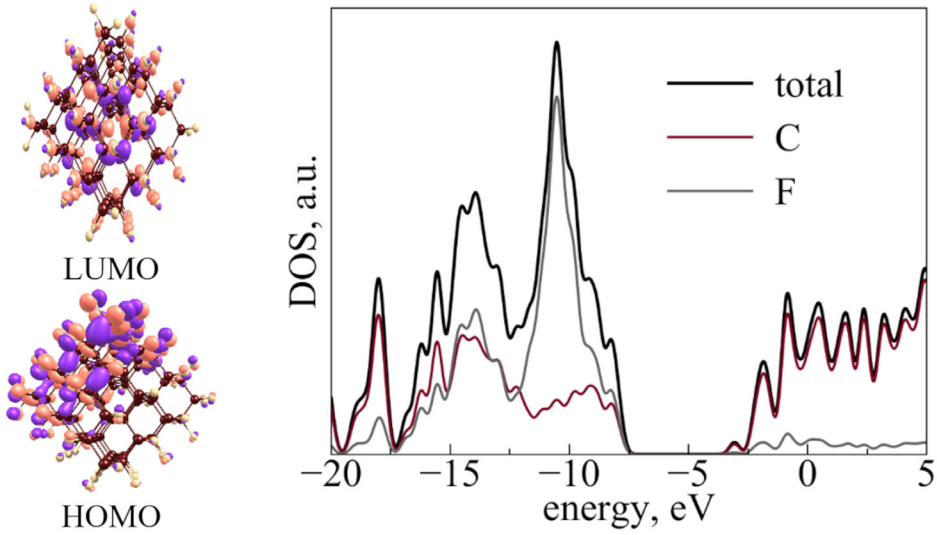

b

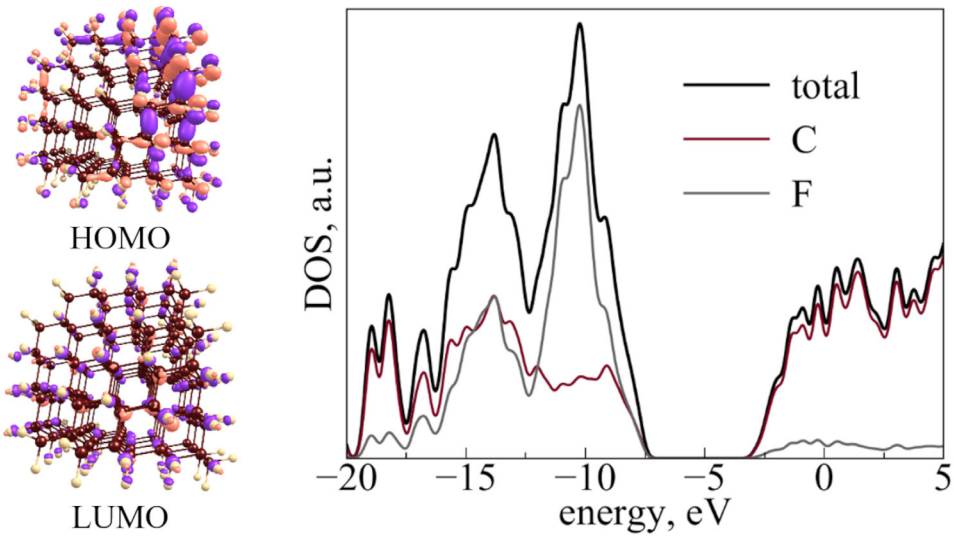

c

Fig. 2. (Color online) Density of electronic states and frontier orbitals of $C_{26}F_{32}$ (a), $C_{84}F_{64}$ (b) and $C_{148}F_{96}$ (c) NDs. All peaks are broadened by gaussians with FWHM = 0.5 eV. Linear scaling is applied to DOS axis.

the polymer model corresponds to the size of the studied diamond nanoparticles. Note that models consisting of 1 to 3 monomers were used in simulations of PMMA/graphene [35] or PMMA/diamond nanothread [36] composites. Finding the optimal adsorption configuration is a non-trivial task, since many configurations are possible. We used the genetic algorithm provided in the ABCluster package for global optimization of the ND + PMMA complex. At the first stage, the parameters of each of the atoms in the molecules were determined using the implemented *topgen* algorithm [37]. We set the population size and number of generations equal to 100 and 200, respectively. Then a pair-wise empirical interatomic interaction is used, calculated on the basis of these parameters. The genetic algorithm based on the empirical intermolecular interaction provides the lowest-energy configurations, which is used as a guess for subsequent more accurate DFT optimization. The resulting equilibrium adsorption configurations are shown in Fig. S2.

The binding energy E_b characterizing the interaction of ND with PMMA is determined as follows:

$$E_b = E(\text{ND} + \text{PMMA}) - E(\text{ND}) - E(\text{PMMA}). \qquad (4)$$

The basis set superposition error (BSSE) is accounted for by using "ghost" atoms, as implemented in TeraChem. According to this technique, the E(ND) and E(PMMA) energies are calculated in the extended electronic basis containing gaussian basic functions from all atoms of the complex. The calculated E_b values and some electronic characteristics of ND + PMMA complexes are summarized in Table 2.

Figure S2 visualizes the partial contributions to the density of electronic states from ND and PMMA. We observe that the frontier orbitals almost do not hybridize. The HOMO and LUMO orbitals are completely localized at PMMA and ND, respectively, see Fig. S2. Therefore, the energy of the HOMO orbital is almost the same for all complexes (about −5.7 eV) and is determined by the PMMA structure, while LUMO is almost equal to the corresponding value for NDs (it is clear from a comparison of Tables 1 and 2). The charge transfer was estimated as the sum of the Lowdin partial charge for all atoms related to ND or PMMA. We observe a slight charge transfer from PMMA to ND, but the total ND charge does not exceed $0.1|e|$. The E_b value is slightly negative only for the smallest NDs. Other NDs possess positive E_b, so the formation of a composite with them is energetically unfavorable. Addition calculation for the smallest complex with the polarized continuum model COSMO implemented in TeraChem with $\varepsilon = 3.7$ yields to of the $E_b = -0.27$ eV, which is very close to the value obtained in a vacuum (−0.30 eV). Thus, the influence of polarization on binding energy proved to be negligible for considered systems. We conclude that the fluorinated ND weakly interacts with PMMA. This is because PMMA has electronegative oxygen atoms that repulse the fluorine shell and does not have suitable H atoms for forming hydrogen bonds. Thus, fluorinated NDs retain their individuality within the composite.

4. Discussion

The functional groups coated the ND determine its interaction with polymers. The desired interaction intensity is dependent on the composite purpose. For example, the strong attraction of the polymer to ND contributes to improved mechanical properties. Weak interaction is undesirable for mechanical applications; however, it provides keeping the electronic and optical properties of the pristine ND, which is useful for photonics. Moreover, coating of ND provides their selectivity with respect to polymers. So, fluorination enhances the interaction through hydrogen bonds, but weakens the bond with other polymers such as PMMA.

Note that many diamond-like nanoarchitectures are being investigated along with classical NDs [38 – 39]. Many of them have outstanding mechanical characteristics comparable to ND [40 – 41]. Thus, we propose three degrees of freedom in the design of functional composites: the type of diamond-like phase forming the nanoparticle, the coating functional groups and the type of matrix polymer. Together with varying the size and concentration of diamond-like particles, this variety provides wide opportunities for the construction of composites for various applications.

5. Conclusion

Our study considers fluorinated NDs within the density functional theory. We found that coated by fluorine results in higher stability of NDs compared to fullerenes, since the former form stronger C-F bonds. An analysis of the density of electronic states and frontier orbitals has shown that fluorine plays an important role in the electronic structure and reactivity of the considered structures. We have identified a weak interaction of NDs with PMMA due to electronegative oxygens contained in PMMA and the absence of hydrogen bonds. Thus, NDs particles retain their electronic and optical characteristics inside the NDs/PMMA composite. In the future, we plan an extensive theoretical study of the influence of different types of coating functional groups on the interaction of NDs with various polymers.

Supplementary material: *The online version of this paper contains supplementary material (Fig. S1 contains equilibrium geometries of the $C_{26}F_{32}$ (a), $C_{84}F_{64}$ (b) and $C_{148}F_{96}$ (c) NDs, Fig. S2 — NDs + PMMA complexes and their total and partial density of electronic states) available free of charge on the journal's website https://lettersonmaterials.com.*

Table 2. Binding energy E_b between ND and PMMA fragment calculated with formula (4). Frontier molecular orbitals HOMO and LUMO for ND + PMMA complexes. The total Lowdin charges of ND and PMMA atoms which characterize the charge transfer are also presented.

	E_b, eV	HOMO, eV	LUMO, eV	gap, eV	q_{ND}	q_{PMMA}
$C_{26}F_{32}$ + PMMA	−0.30	−5.72	−1.83	3.89	0.07	−0.07
$C_{84}F_{64}$ + PMMA	0.66	−5.68	−3.18	2.50	0.10	−0.10
$C_{148}F_{96}$ + PMMA	2.00	−5.68	−2.86	2.82	0.10	−0.10

References

1. N. Nunn, M. Torelli, G. McGuire, O. Shenderova, Nanodiamond: A high impact nanomaterial, Current Opinion in Solid State and Materials Science 21 (2017) 1–9.
2. A. S. Barnard, S. P. Russo, I. K. Snook, Size dependent phase stability of carbon nanoparticles: Nanodiamond versus fullerenes, J. Chem. Phys. 118 (2003) 5094 – 5097.
3. I. V. Popov, A. L. Görne, A. L. Tchougréeff, R. Dronskowski, Relative stability of diamond and graphite as seen through bonds and hybridizations, Phys. Chem. Chem. Phys. 21 (2019) 10961–10969.
4. Q. Jiang, Z. P. Chen, Thermodynamic phase stabilities of nanocarbon, Carbon 44 (2006) 79 – 83.
5. R. Ye, X. Han, D. V. Kosynkin, Y. Li, C. Zhang, B. Jiang, A. A. Martí, J. M. Tour, Laser-Induced Conversion of Teflon into Fluorinated Nanodiamonds or Fluorinated Graphene, ACS Nano 12 (2018) 1083 –1088.
6. V. N. Khabashesku, V. P. Filonenko, R. Kh. Bagramov, A. S. Anokhin, E. V. Kukueva, O. V. Kuznetsov, Impact of surface fluorination on phase stability of nanodiamond particles and inter-granular bonding in polycrystalline diamond under HPHT conditions, Diamond and Related Materials 112 (2021) 108247.
7. E. M. Zagrebina, A. V. Generalov, A. Yu. Klyushin, K. A. Simonov, N. A. Vinogradov, M. Dubois, L. Frezet, N. Mårtensson, A. B. Preobrajenski, A. S. Vinogradov, Comparative NEXAFS, NMR, and FTIR Study of Various-Sized Nanodiamonds: As-Prepared and Fluorinated, J. Phys. Chem. C 119 (2015) 835 – 844.
8. V. Nesvizhevsky, U. Köster, M. Dubois, N. Batisse, L. Frezet, A. Bosak, L. Gines, O. Williams, Fluorinated nanodiamonds as unique neutron reflector, Carbon 130 (2018) 799 – 805.
9. R. Romero-Aburto, Tharangattu. N. Narayanan, Y. Nagaoka, T. Hasumura, T. M. Mitcham, T. Fukuda, P. J. Cox, R. R. Bouchard, T. Maekawa, D. S. Kumar, S. V. Torti, S. A. Mani, P. M. Ajayan, Fluorinated Graphene Oxide; a New Multimodal Material for Biological Applications, Advanced Materials 25 (2013) 5632 – 5637.
10. H.-H. Huang, H. Tsai, R. Raja, S.-L. Lin, D. Ghosh, C.-H. Hou, J.-J. Shyue, S. Tretiak, W. Chen, K.-F. Lin, W. Nie, L. Wang, Robust Unencapsulated Perovskite Solar Cells Protected by a Fluorinated Fullerene Electron Transporting Layer, ACS Energy Lett. 6 (2021) 3376 – 3385.
11. M. K. A. Mohammed, A. K. Al-Mousoi, A. Kumar, A. R. J. Katae, O. A. Khaleel, D. S. Ahmed, M. K. Hossain, Fluorinated carbon nanotubes: a low-cost hole transport layer for perovskite solar cells, J. Mater. Sci. 58 (2023) 11748 –11760.
12. R. A. Borse, M. B. Kale, S. H. Sonawane, Y. Wang, Fluorographene and Its Composites: Fundamentals, Electrophysical Properties, DFT Studies, and Advanced Applications, Adv. Funct. Materials 32 (2022) 2202570.
13. E. B. Kalika, K. P. Katin, A. I. Kochaev, S. Kaya, M. Elik, M. M. Maslov, Fluorinated carbon and boron nitride fullerenes for drug Delivery: Computational study of structure and adsorption, J. Mol. Liquids 353 (2022) 118773.
14. O. Bolshakova, V. Lebedev, E. Mikhailova, O. Zherebyateva, L. Aznabaeva, V. Burdakov, Y. Kulvelis, N. Yevlampieva, A. Mironov, I. Miroshnichenko, S. Sarantseva, Fullerenes on a Nanodiamond Platform Demonstrate Antibacterial Activity with Low Cytotoxicity, Pharmaceutics 15 (2023) 1984.
15. V. P. Filonenko, V. N. Khabashesku, Prospects for the Use of Fluorinated Nanodiamonds in the Synthesis of Superhard Composites, Nanotechnol. Russia 17 (2022) 529 – 533.
16. V. N. Khabashesku, V. P. Filonenko, R. K. Bagramov, I. P. Zibrov, Diamond Composites Produced from Fluorinated Mixtures of Micron-Sized and Nanodiamonds by Metal Infiltration, Materials 15 (2022) 4936.
17. C. Laube, F. Yang, M. Naumann, J. Griebel, A. Prager, A. Lotnyk, P. Lorenz, K. Zimmer, U. Helmstedt, B. Abel, Nanodiamond-Polymer Composites for Decreased Laser Ablation Thresholds, ACS Appl. Nano Mater. 7 (2024) 8842 – 8853.
18. E. Hadden, M. Fally, Y. Iso, T. Jenke, J. Klepp, A. Kume, K. Umemoto, Y. Tomita, Holographic nanodiamond — polymer composite grating with unprecedented slow-neutron refractive index modulation amplitude, Appl. Phys. Lett. 124 (2024) 071901.
19. O. V. Lebedev, T. S. Kurkin, E. K. Golubev, A. L. Vasiliev, A. K. Gatin, G. P. Goncharuk, A. N. Ozerin, Detonation Synthesis Nanodiamond Soot as a Promising Filler for Polymer Composites, C 8 (2022) 69.
20. F. Pan, M. Khan, L. Tiehu, E. Javed, A. Hussain, A. Zada, D. Alei, Z. Wahab, Effect of nanodiamond particles on the structure, mechanical, and thermal properties of polymer embedded ND/PMMA composites, Journal of Polymer Engineering 42 (2022) 795 – 807.
21. S. M. Fouda, M. M. Gad, P. Ellakany, M. A. Al Ghamdi, S. Q. Khan, S. Akhtar, M. S. Ali, F. A. Al-Harbi, Flexural Properties, Impact Strength, and Hardness of Nanodiamond-Modified PMMA Denture Base Resin, Int. J. Biomaterials 2022 (2022) 1–10.
22. S. M. Fouda, M. M. Gad, P. Ellakany, M. A. Al Ghamdi, S. Q. Khan, S. Akhtar, D. M. Al Eraky, F. A. Al-Harbi, Effect of Low Nanodiamond Concentrations and Polymerization Techniques on Physical Properties and Antifungal Activities of Denture Base Resin, Polymers 13 (2021) 4331.
23. C. Wang, X. Cao, J. Tian, F. Yu, F. Jiang, K. Ren, Significantly enhanced energy density of nanodiamond/polyimide composites at high temperatures with ultralow nanodiamond contents, Sci. China Technol. Sci. 66 (2023) 956 – 965.
24. M. M. Gad, M. S. Ali, A. M. Al-Thobity, Y. A. Al-Dulaijan, M. E. Zayat, A.-N. M. Emam, S. Akhtar, S. Q. Khan, F. A. Al-Harbi, S. M. Fouda, Polymethylmethacrylate Incorporating Nanodiamonds for Denture Repair: *In Vitro* Study on the Mechanical Properties, Eur. J. Dent. 16 (2022) 286 – 295.
25. A. Kausar, Nanodiamond integrating poly (methyl methacrylate) nanocomposites intending for technological innovations, Materials Research Innovations 25 (2021) 310 – 319.
26. E. B. Kalika, N. V. Bondarev, K. P. Katin, A. I. Kochaev,

A. A. Grekova, S. Kaya, Y. A. Bauetdinov, M. M. Maslov, Adsorption of 40 low molecular weight drugs on pristine and fluorinated C_{60} fullerenes: *Ab initio*, statistical and neural networks analysis, J. Mol. Liquids 377 (2023) 121559.
27. A. Chatzigoulas, K. Karathanou, D. Dellis, Z. Cournia, NanoCrystal: A Web-Based Crystallographic Tool for the Construction of Nanoparticles Based on Their Crystal Habit, J. Chem. Inf. Model. 58 (2018) 2380 – 2386.
28. J. Zhang, M. Dolg, ABCluster: the artificial bee colony algorithm for cluster global optimization, Phys. Chem. Chem. Phys. 17 (2015) 24173 – 24181.
29. E. Caldeweyher, C. Bannwarth, S. Grimme, Extension of the D3 dispersion coefficient model, J. Chem. Phys. 147 (2017) 034112.
30. J. Kästner, J. M. Carr, T. W. Keal, W. Thiel, A. Wander, P. Sherwood, DL-FIND: An Open-Source Geometry Optimizer for Atomistic Simulations, J. Phys. Chem. A 113 (2009) 11856 –11865.
31. A. V. Titov, I. S. Ufimtsev, N. Luehr, T. J. Martinez, Generating Efficient Quantum Chemistry Codes for Novel Architectures, J. Chem. Theory Comput. 9 (2013) 213 – 221.
32. T. Lu, F. Chen, Multiwfn: A multifunctional wavefunction analyzer, J. Comput. Chem. 33 (2012) 580 – 592.
33. B. Fu, Surface Energy of Diamond Cubic Crystals and Anisotropy Analysis Revealed by Empirical Electron Surface Models, Adv. Mater. 8 (2019) 61.
34. M. Dubois, K. Guérin, A. Hamwi, A. Vinogradov, Nature of C-F Bonds in Fluorinated Carbons, in O. Boltalina and T. Nakajima (Eds.), New Fluorinated Carbons: Fundamentals and Applications, Elsevier, Amsterdam, 2017, pp. 215 – 243.
35. E. López-Chávez, A. Garcia-Quiroz, J. A. I. Díaz-Góngora, J. A. López-Barrera, J. A. Mendoza-Espinoza, Y. A. Peña-Castañeda, F. de Landa Castillo-Alvarado, Effect of graphene on the key electrical, optical, and magnetic properties of polymethylmethacrylate: a study based on molecular modeling, J. Mol. Model. 30 (2024) 375.
36. B. B. Yin, J. S. Huang, W. M. Ji, K. M. Liew, Exploring frictional performance of diamond nanothread reinforced polymer composites from the atomistic simulation and density functional theory, Carbon 200 (2022) 10 – 20.
37. J. Zhang, M. Dolg, Global optimization of clusters of rigid molecules using the artificial bee colony algorithm, Phys. Chem. Chem. Phys. 18 (4) (2016) 3003 – 3010.
38. J. A. Baimova, An Overview of Mechanical Properties of Diamond-like Phases under Tension, Nanomaterials 14 (2024) 129.
39. V. A. Greshnyakov, Hexagonal Diamond: Theoretical Study of Methods of Fabrication and Experimental Identification, JETP Lett. 117 (2023) 306 – 312.
40. J. A. Baimova, L. Kh. Galiakhmetova, R. R. Mulyukov, Diamond-like structures under hydrostatic loading: Atomistic simulation, Comput. Mater. Sci. 192 (2021) 110301.
41. L. Kh. Rysaeva, J. A. Baimova, S. V. Dmitriev, D. S. Lisovenko, V. A. Gorodtsov, A. I. Rudskoy, Elastic properties of diamond-like phases based on carbon nanotubes, Diamond and Related Materials 97 (2019) 107411.